


Chloroplast-derived photo-oxidative stress causes changes in H_2O_2 and E_{GSH} in other subcellular compartments

José Manuel Ugalde ¹, Philippe Fuchs ^{1,2}, Thomas Nietzel ², Edoardo A. Cutolo ^{3,†}, Maria Homagk ¹, Ute C. Vothknecht ³, Loreto Holuigue ⁴, Markus Schwarzländer ², Stefanie J. Müller-Schüssele ¹ and Andreas J. Meyer ^{1,*‡}

¹ Institute of Crop Science and Resource Conservation (INRES), University of Bonn, D-53113 Bonn, Germany

² Institute of Plant Biology and Biotechnology, University of Münster, D-48143 Münster, Germany

³ Institute of Cellular and Molecular Botany (IZMB), University of Bonn, D-53115 Bonn, Germany

⁴ Departamento de Genética Molecular y Microbiología, Facultad de Ciencias Biológicas, Pontificia Universidad Católica de Chile, Santiago 8331150, Chile

*Author for communication: andreas.meyer@uni-bonn.de

†Present address: Laboratory of Photosynthesis and Bioenergy, Department of Biotechnology, University of Verona, Strada le Grazie 15, 37134 Verona, Italy.

‡Senior author.

J.M.U., U.C.V., L.H., S.J.M.-S., and A.J.M. conceived and designed the experiments; J.M.U. and M.H. performed the experiments; T.N. and E.A.C. contributed new constructs and plant lines; J.M.U., P.F., M.S., S.J.M.-S., and A.J.M. analyzed the data; J.M.U., S.J.M.-S., and A.J.M. wrote the manuscript with contributions from all authors.

The author responsible for distribution of materials integral to the findings presented in this article in accordance with the policy described in the Instructions for Authors (<https://academic.oup.com/plphys/pages/general-instructions>) is: Andreas J. Meyer (andreas.meyer@uni-bonn.de).

Abstract

Metabolic fluctuations in chloroplasts and mitochondria can trigger retrograde signals to modify nuclear gene expression. Mobile signals likely to be involved are reactive oxygen species (ROS), which can operate protein redox switches by oxidation of specific cysteine residues. Redox buffers, such as the highly reduced glutathione pool, serve as reservoirs of reducing power for several ROS-scavenging and ROS-induced damage repair pathways. Formation of glutathione disulfide and a shift of the glutathione redox potential (E_{GSH}) toward less negative values is considered as hallmark of several stress conditions. Here we used the herbicide methyl viologen (MV) to generate ROS locally in chloroplasts of intact *Arabidopsis thaliana* seedlings and recorded dynamic changes in E_{GSH} and H_2O_2 levels with the genetically encoded biosensors Grx1-roGFP2 (for E_{GSH}) and roGFP2-Orp1 (for H_2O_2) targeted to chloroplasts, the cytosol, or mitochondria. Treatment of seedlings with MV caused rapid oxidation in chloroplasts and, subsequently, in the cytosol and mitochondria. MV-induced oxidation was significantly boosted by illumination with actinic light, and largely abolished by inhibitors of photosynthetic electron transport. MV also induced autonomous oxidation in the mitochondrial matrix in an electron transport chain activity-dependent manner that was milder than the oxidation triggered in chloroplasts by the combination of MV and light. In vivo redox biosensing resolves the spatiotemporal dynamics of compartmental responses to local ROS generation and provides a basis for understanding how compartment-specific redox dynamics might operate in retrograde signaling and stress acclimation in plants.

Introduction

Communication between different subcellular compartments of plant cells is fundamental to establish and sustain cooperative functioning and to acclimate to diverse environmental conditions. Since most plastidial and mitochondrial proteins are encoded in the nuclear genome, retrograde signals from the organelles to the nucleus are essential to adjust organelle function by coordinating the expression of nuclear and organellar genomes (Van Aken et al., 2016; de Souza et al., 2017; Dietz et al., 2019). Communication between the endosymbiotic organelles and the nucleus is likely to involve the cytosol as the intermediate compartment. However, chloroplasts can also make direct physical contact with the nuclear envelope via stromules, which has been suggested to mediate signaling (Caplan et al., 2015; Erickson et al., 2017; Exposito-Rodriguez et al., 2017). Physical interaction also occurs between different organelles and may facilitate efficient exchange of metabolites and information (Pérez-Sancho et al., 2016; Perico and Sparkes, 2018).

Reactive oxygen species (ROS), such as hydrogen peroxide (H_2O_2), have emerged as signaling molecules in plants and their roles in early signaling events initiated by cellular metabolic perturbation and environmental stimuli are established (Waszczak et al., 2018; Smirnov and Arnaud, 2019). During unfavorable environmental conditions, superoxide ($\text{O}_2^{\cdot-}$) is produced at an increased rate by the electron transport chains (ETCs) in chloroplasts and mitochondria. $\text{O}_2^{\cdot-}$ is rapidly converted to H_2O_2 and molecular oxygen (O_2) by superoxide dismutases (SODs). H_2O_2 can be further detoxified through a set of peroxidases, including peroxiredoxins (PRX; Liebthal et al., 2018) several glutathione S-transferases (Sylvestre-Gonon et al., 2019; Ugalde et al., 2020b), glutathione peroxidase (GPX)-like enzymes (Attacha et al., 2017), and ascorbate peroxidases (APX). The latter operates as part of the ascorbate-glutathione cycle in the plastid stroma, mitochondrial matrix, peroxisomes, and cytosol (Foyer and Noctor, 2005; Narendra et al., 2006). The transient drain of electrons from the local glutathione redox buffer causes a concomitant increase in glutathione disulfide (GSSG) and hence a change in the glutathione redox potential (E_{GSH} ; Marty et al., 2009; Bangash et al., 2019; Nietzel et al., 2019; Wagner et al., 2019). Intracellular H_2O_2 levels reached under stress conditions can affect cellular redox regulation leading to the oxidation of protein thiols (Dietz et al., 2016). H_2O_2 was shown to diffuse across the chloroplast envelope even at low concentrations, and it has been estimated that about 5% of the total ROS produced in high light leave the chloroplast (Mubarakshina et al., 2010). Those properties contributed to the suggestion of H_2O_2 to operate as a messenger in signaling processes arising from the organelles. Moreover, direct transfer of H_2O_2 from a subpopulation of chloroplasts localized in close proximity to the nucleus itself was recently found to mediate photosynthetic control over gene expression in *Nicotiana benthamiana* leaves (Caplan et al., 2015; Exposito-Rodriguez et al., 2017).

ROS production at specific sites of the photosynthetic ETC (pETC) can be artificially enhanced by using inhibitors and redox catalysts. Among these, the herbicide methyl viologen (MV) acts by re-directing electrons from photosystem I (PSI) to O_2 and thereby enhancing the production of $\text{O}_2^{\cdot-}$ (Scarpeci et al., 2008). Based on its mechanism, MV is also useful as an experimental cue to induce photo-oxidative stress in photosynthetic organisms. In mammals and other nonphotosynthetic organisms, MV induces the generation of $\text{O}_2^{\cdot-}$ by re-directing electrons from complex I of the mitochondrial ETC (mETC) to O_2 (Cochemé and Murphy, 2008), suggesting that current models to study retrograde signaling are likely to be more complex than previously expected and involve additional subcellular sites (Cui et al., 2019; Shapiguzov et al., 2019). Steady-state measurements in cotyledons of Arabidopsis seedlings have previously shown that MV can induce oxidation in both cytosol and mitochondria in the absence of illumination (Schwarzländer et al., 2009).

Chemical probes for detecting ROS in living systems, such as 2',7'-dihydrodichlorofluorescein diacetate ($\text{H}_2\text{DCF-DA}$) are typically converted to a fluorescent product through reaction with ROS and accumulate in tissues with different specificities for distinct forms of ROS (Fichman et al., 2019). While these dyes provide evidence for redox processes and ROS formation, a potential drawback is that those probes act irreversibly by generating an accumulative signal rather than a reversible, dynamic response. Further, their lack of unambiguous subcellular localization and chemical specificity make it frequently difficult to draw mechanistic conclusions. During the last decades, genetically encoded biosensors have provided insights in the field of cell physiology by being targetable to specific subcellular compartments and enabling dynamic measurements. Among them, Grx1-roGFP2 for sensing E_{GSH} (Marty et al., 2009) and roGFP2-Orp1 for sensing transient changes in H_2O_2 (Nietzel et al., 2019); the latter being based on a redox relay between the GPX-like enzyme oxidant receptor peroxidase-1 (Orp1; syn. Gpx3) from yeast (*Saccharomyces cerevisiae*) and roGFP2 (Gutscher et al., 2009). These sensors have become instrumental to monitor the dynamics of oxidative signals in real-time in a wide range of organisms, including plants. Similarly, probes of the HyPer family, which exploit the H_2O_2 -sensitive bacterial transcription factor OxyR for their response, can report on local alterations in H_2O_2 concentrations (Bilan and Belousov, 2018; Pak et al., 2020).

Despite compelling evidence for the signaling functions of H_2O_2 , it is neither known how H_2O_2 concentrations and the redox buffers dynamically respond to increased ROS production in chloroplasts nor how much other organelles contribute to a cumulative oxidation in the cytosol. Here, we targeted two different roGFP2-based biosensors to the stroma of the chloroplasts; the cytosol and the matrix of the mitochondria to live monitor the local E_{GSH} and H_2O_2 dynamics specifically in those three compartments. We investigated the dynamic subcellular responses to primary oxidative events triggered by MV, light or a combination of

both. To dissect the contribution of chloroplasts and mitochondria in the MV-induced overall oxidation, the respective ETCs were blocked using ETC-specific inhibitors acting at early steps of electron transport.

Results

Spectral properties of roGFP2-based probes in planta

To visualize changes of E_{GSH} or H_2O_2 levels in chloroplasts, cytosol and mitochondria, we selected previously published Arabidopsis reporter lines with roGFP2 linked to Grx1 or Orp1, respectively (Marty et al., 2009; Park et al., 2013; Albrecht et al., 2014; Nietzel et al., 2019). Since no roGFP2-Orp1 reporter line for H_2O_2 sensing in the plastid was available, we generated this line de novo (Supplemental Figure S1). Subcellular localization of all reporter constructs was verified side-by-side in 7-d-old seedlings by confocal microscopy (Figure 1, A–S, left panels and Supplemental Figure S1). Plants of the same age were used to systematically corroborate the in vivo excitation spectra of both redox sensors in all three compartments of intact seedlings. Sensor response and the dynamic spectroscopic response range were assessed by recording the fluorescence of seedlings immersed in imaging buffer using a fluorescence multiwell plate reader. Fluorescence spectra were collected for nontreated seedlings and seedlings incubated with either 20 mM 1,4-dithiothreitol (DTT) for complete reduction or with 100 mM H_2O_2 for complete oxidation of the sensors in situ (Figure 1, A–F, right panels). Sensor fluorescence intensities were sufficiently high to be clearly distinguishable from background fluorescence with a suitable signal-to-noise ratio for in situ readings (Supplemental Figure S2). Fully reduced Grx1-roGFP2 (roGFP2-Grx1 in the case of the mitochondria) or roGFP2-Orp1 showed low excitation at 400 nm and a pronounced excitation peak close to 488 nm in all compartments. Probe oxidation led to the appearance of a second distinct excitation peak close to 400 nm, while excitation at 488 nm was decreased (Figure 1, A–F, right panels; Supplemental Figure S2). The spectral behavior of both probes in planta was consistent with the spectra of the purified roGFP2 in vitro (Figure 1H). These data validate that changes in the redox state of both roGFP2-based sensor variants can be reliably visualized and recorded in chloroplast stroma, cytosol, and mitochondrial matrix using plate reader-based fluorimetry (Nietzel et al., 2019; Wagner et al., 2019).

Real-time monitoring of E_{GSH} and H_2O_2 dynamics in Arabidopsis in response to externally imposed oxidative stress

To further validate the responsiveness of both probes in planta, 7-d-old Arabidopsis seedlings expressing cytosol-targeted Grx1-roGFP2 or roGFP2-Orp1 were exposed to different concentrations of H_2O_2 to impose oxidative stress (Figure 2). Changes in the redox state of both sensors were followed in real-time by exciting roGFP2 at 410 nm

and 480 nm in wild-type (WT) expressing the cytosolic-targeted roGFP2-based sensors. The recorded fluorescence of roGFP2 in the individual channels (410 nm and 480 nm) showed an immediate response in opposite directions upon addition of H_2O_2 , with an increase of the 410 nm channel while the fluorescence excited at 480 nm decreased (Figure 2, D and E, left panels; Supplemental Figure S3, A–E). After reaching a peak of oxidation, a gradual recovery of both channels towards the starting values prior to addition of H_2O_2 occurred over a period of about 4 h (Figure 2, D and E; Supplemental Figure S3). For analysis, the 410 nm/480 nm fluorescence ratio was calculated and used as a measure for sensor oxidation and hence as an indicator for relative changes in E_{GSH} and H_2O_2 , respectively. Starting from low ratio values in nontreated seedlings, the addition of H_2O_2 caused a rapid increase of the 410 nm/480 nm fluorescence ratio followed by a gradual decline over several hours (Figure 2, D and E, right panels). In WT plants, the speed of oxidation was independent of the amount of H_2O_2 , but the maximum peak height increased with increasing concentrations of H_2O_2 (Figure 2, D and E). Maximum fluorescence ratio values were reached between 8 mM and 10 mM exogenous H_2O_2 application for both sensors (Figure 2C). In all experiments, the minimum and maximum fluorescence ratios of the respective probes in their fully oxidized and fully reduced state were determined after each experiment as shown for the cytosolic roGFP2-Orp1 sensor (Supplemental Figure S3F). To further validate the sensor response and to show that the recovery of the redox status is indeed a true reflection of gradual H_2O_2 degradation, we also measured the oxidation of Grx1-roGFP2 and roGFP2-Orp1 in the cytosol of mutants deficient in catalase 2 (CAT2), which is the most abundant catalase in photosynthetic tissues of Arabidopsis and has a very fast turnover rate (Mhamdi et al., 2010). In *cat2* seedlings, the sensor was initially almost fully reduced and the sensor fluorescence ratio increased with a similar rate as in WT seedlings. Like in WT, the maximum fluorescence ratio reached in *cat2* was dependent on the amount of H_2O_2 added to the incubation medium (Figure 2, F and G). Consistent with our hypothesis that CAT2 plays a major role in handling large H_2O_2 flux, the subsequent decrease of fluorescence ratios occurred only slowly and was completely abolished in seedlings incubated in 10 mM H_2O_2 (Figure 2, F and G, right panels).

The impact of MV on sensor oxidation is most pronounced in chloroplasts

After confirming the fast and concentration-dependent response of the sensors towards H_2O_2 treatments in vivo, we evaluated the sensitivity of the plate reader-based fluorimetry setup to detect redox changes induced by MV. For this purpose, 7-d-old seedlings expressing Grx1-roGFP2, roGFP2-Grx1, or roGFP2-Orp1 targeted to plastid stroma, the cytosol or the mitochondrial matrix were treated with different concentrations of MV and sensor fluorescence was continuously recorded in plate reading mode for 6 h (Figure 3). In

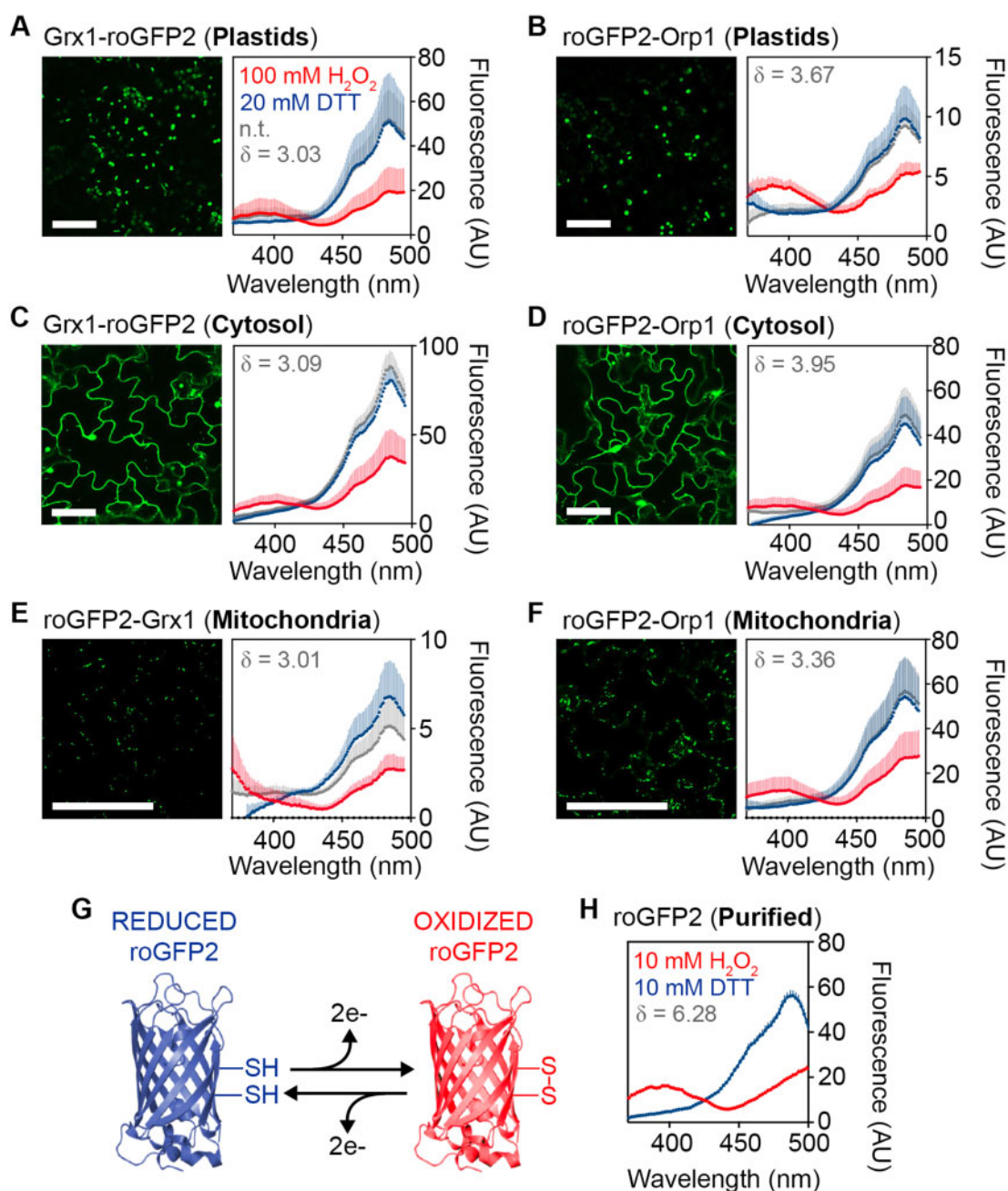


Figure 1 Subcellular localization and spectral behavior of E_{GSH} and H_2O_2 sensors in Arabidopsis. A–F (left panels), Confocal microscopy images of leaf epidermal cells from 7-d-old seedlings stably expressing Grx1-roGFP2, roGFP2-Grx1, or roGFP2-Orp1 targeted to plastids (A, B), cytosol (C, D), or mitochondria (E, F). All images show roGFP2 fluorescence recorded with $\lambda_{\text{ex}} = 488$ nm and $\lambda_{\text{em}} = 505\text{--}530$ nm. Bars, 50 μm . A–F (right panels), Grx1-roGFP2, roGFP2-Grx1, or roGFP2-Orp1 fluorescence excitation spectra for nontreated seedlings (n.t., gray), and after reduction with 20 mM DTT (blue) or oxidation with 100 mM H_2O_2 (red). All spectra were recorded on a plate reader from 7-d-old seedlings with emission at 520 ± 5 nm and using the same gain for all lines. The curves show the mean of the fluorescence in AU \pm SD, with $n \geq 3$ biological replicates, where each replicate is an independent pool of 4–5 seedlings. All spectra were corrected for the autofluorescence measured in nontransformed control seedlings (see [Supplemental Figure S1](#)). The dynamic range (δ) for the maximum change of the fluorescence ratio between the fully oxidized and fully reduced sensor was calculated from the fluorescence collected after sensor excitation at 410 and 480 nm. G, Schematic model of roGFP2 structure highlighting the disulfide bond formation upon reversible oxidation. H, Excitation spectrum of purified roGFP2 measured under similar conditions as the seedlings. To achieve full reduction and full oxidation, the purified protein was incubated in 10 mM DTT or 10 mM H_2O_2 , respectively. Mean \pm SD, $n = 6$.

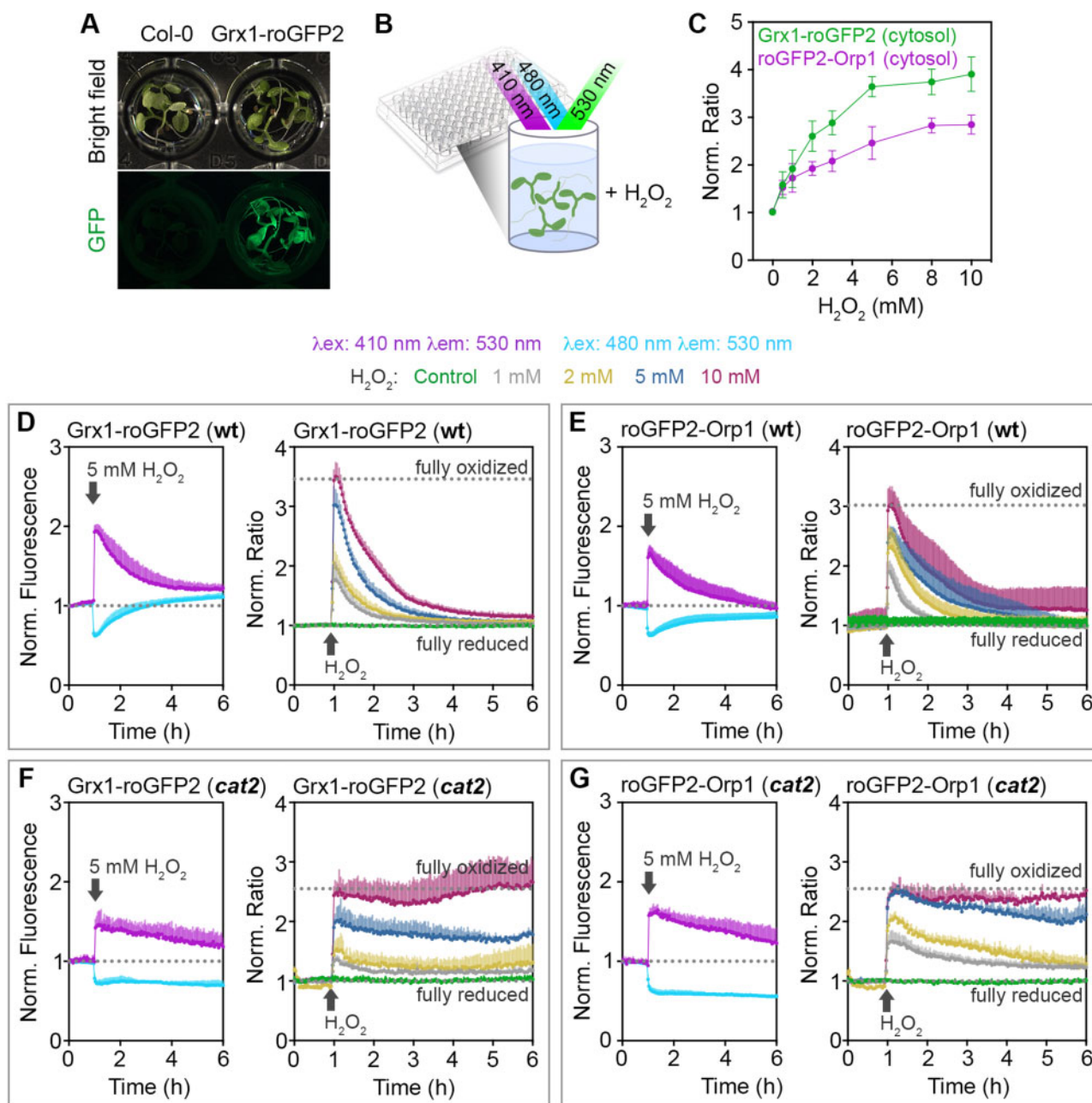


Figure 2 Real-time monitoring of cytosolic Grx1-roGFP2 and roGFP2-Orp1 redox changes upon imposition of oxidative stress in planta. A, Pools of 7-d-old seedlings (4–5 per well) expressing Grx1-roGFP2 or roGFP2-Orp1 in the cytosol were placed in a 96-well plate. B, The redox state of the sensors was measured as the roGFP2 fluorescence after sequential excitation at $\lambda_{ex} = 410 \pm 5$ nm and $\lambda_{ex} = 480 \pm 5$ nm. Fluorescence was always recorded at $\lambda_{em} = 530 \pm 20$ nm. C, Normalized ratio between the fluorescence intensities of both channels in plants expressing cytosol-targeted Grx1-roGFP2 or roGFP2-Orp1 after treatment with the indicated H₂O₂ concentrations. D–G (left panels), Time-resolved fluorescence recordings for the two independent channels after addition of 5 mM H₂O₂ at $t = 1$ h to WT plants (D, E) and *cat2* (F, G). Both curves are normalized to their initial values before imposed oxidation (dotted lines). D–G (right panels), Fluorescence ratio values calculated to the original fluorescence in both channels in response to different concentrations of H₂O₂ on WT (D, E) and *cat2* (F, G) lines. For control samples, only buffer was added. The curves show the mean ratio + SD from $n = 4$ biological replicates, where each replicate is an independent pool of 4–5 seedlings. The ratio values are normalized to the original ratio values before addition of H₂O₂. The experiment was repeated three times with similar results. Dotted lines (D–G, right panels) indicate minimum and maximum ratio values measured from the same wells at the end of the experiment during incubation in 100 mM H₂O₂ for full oxidation and in 20 mM DTT for full reduction of the probes (see Supplemental Figure S3).

chloroplasts, the oxidation of both probes gradually increased over time, with roGFP2-Orp1 showing a faster oxidation immediately after MV treatments compared to Grx1-roGFP2 (Figure 3, A–C; Supplemental Figure S4, A and B). In

contrast to the response in chloroplasts, the fluorescence ratios of cytosolic Grx1-roGFP2 and roGFP2-Orp1 remained low suggesting that both probes remained largely reduced under the same treatments (Figure 3, D–F; Supplemental

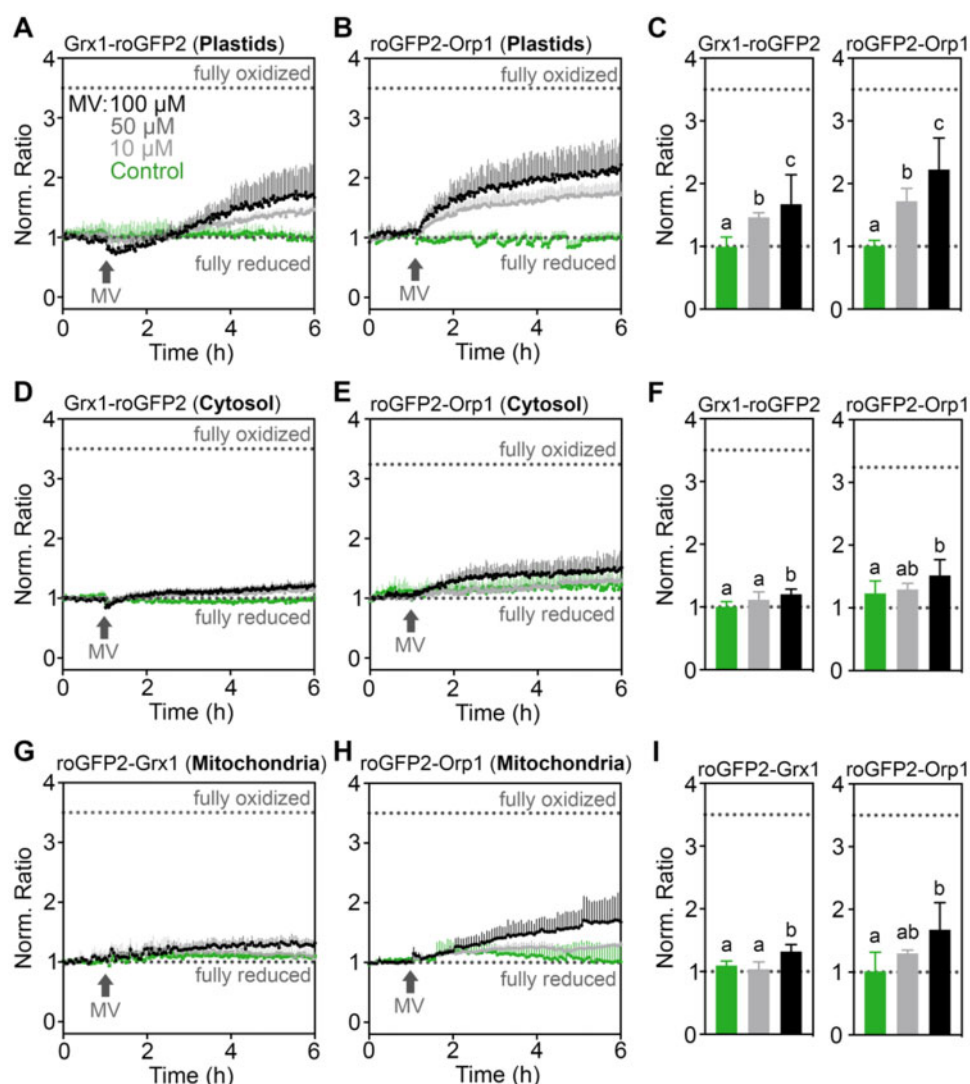


Figure 3 Real-time monitoring of the E_{GSH} and H_2O_2 sensors upon MV-induced oxidation in planta. A–I, Seven-day-old seedlings stably expressing Grx1-roGFP2, roGFP-Grx1, or roGFP2-Orp1 targeted to the cytosol, plastids, or mitochondria were placed in a 96-well plate with imaging buffer. After 1 h, MV was added to a final concentration indicated in panel A. In control samples (green), only buffer was added to maintain a uniform total buffer volume throughout the experiments. Ratio values were calculated from the fluorescence recorded by sequential excitation of probes at 410 ± 5 nm and 480 ± 5 nm, and normalized to the initial ratio at 0 h. Fluorescence was always recorded at 530 ± 20 nm. Dotted lines indicate ratio values measured from the same wells at the end of each experiment after incubation in 20 mM DTT for full reduction or 100 mM H_2O_2 for full oxidation of the probes. C, F, I, Endpoint ratio values at 6 h extracted from panels (A, B, D, E, G, and H). Mean ratios + SD, $n \geq 3$ biological replicates, where each replicate is an independent pool of 4–5 seedlings. Different letters indicate statistical differences between ratios after log₁₀ transformation, according to one-way ANOVA with Tukey's multiple comparison test ($P < 0.05$). Data for individual excitation channels are presented in [Supplemental Figure S4](#).

[Figure S4, C and D](#)). Despite the slow oxidation, ratio values 5 h after addition of MV were higher than in control seedlings. In mitochondria, both sensors revealed a gradual oxidation after the addition of 100 μ M MV, roGFP2-Orp1 ratio increased more strongly during the first 5 h after the addition of MV than roGFP2-Grx1 ([Figure 3, G–I](#); [Supplemental Figure S4, E and F](#)). Detection of MV-induced oxidative stress was also detected through labeling with H_2DCF -DA as an orthogonal approach ([Supplemental Figure S5](#)). H_2DCF -DA provides an accumulative fluorescent readout integrating ROS-mediated oxidation over time. Measurements of

the MV-triggered redox dynamics with roGFP2-based sensors offers the opportunity to resolve temporal dynamics of ROS flux. In none of the experiments conducted initially, however, a reversal of the increase in fluorescence ratio was observed. This suggests that under conditions of the chosen experimental design MV causes sustained oxidation that cannot be counteracted by the different subcellular antioxidant systems. To further test whether the xenon flash light used for roGFP2 excitation in the plate reader was sufficient to cause the oxidation of roGFP2 by photo-oxidative effects, we increased the cycle time for fluorescence readings from

3 to 60 min. Decreased excitation frequency abolished the detectable roGFP2-Orp1 oxidation in chloroplasts and the cytosol, which is consistent with light-dependency of MV-mediated ROS generation in chloroplasts (Supplemental Figure S6). In mitochondria, however, even only a single excitation event per hour already led to slight oxidation of roGFP2-Orp1 5 h after addition of MV. Oxidation in the mitochondria corresponds with flash frequencies, validating its illumination-dependence.

Continuous light enhances MV-induced oxidation in chloroplasts, cytosol, and mitochondria

The more pronounced oxidation induced by MV in chloroplasts compared to the cytosol and mitochondria (Figure 3) was related to the unavoidable intermittent illumination during data collection (Supplemental Figure S6). While this primary oxidation in chloroplasts was exploited for the following experiments, the results would only be physiologically meaningful as long as the seedlings do not get seriously damaged over the course of the experiment, especially when illuminated at high frequencies or even intermittent periods of continuous light. To test whether MV in combination with illumination had obvious effects on plant viability, Arabidopsis seedlings that had been exposed to excitation light every 3 min for a 15-h fluorescence recording were taken out of the plates and transferred to agar plates for phenotype documentation. All seedlings that had been repeatedly illuminated with excitation light were still green and fully turgid irrespective of the MV concentration (Supplemental Figure S7A). Even if seedlings were illuminated with constant actinic light with an intensity of $200 \mu\text{mol m}^{-2} \text{s}^{-1}$ for 1 h after the first 2 h of the 15-h time course, no obvious toxic effect of MV could be recognized macroscopically (Supplemental Figure S7B). In contrast, seedlings kept under constant actinic light with an intensity of $200 \mu\text{mol m}^{-2} \text{s}^{-1}$ for 15 h showed loss of chlorophyll already with $10 \mu\text{M}$ MV and even more seriously with $100 \mu\text{M}$ MV, which caused complete bleaching (Supplemental Figure S7C).

After confirming that 1-h illumination outside the plate reader does not severely damage the seedlings, we used this regime to further boost ROS formation in chloroplasts (Figure 4, A–I). The 1-h illumination with constant actinic light with an intensity of $200 \mu\text{mol m}^{-2} \text{s}^{-1}$ caused a transient increase in the fluorescence ratio of both sensors targeted to chloroplasts and mitochondria in untreated control seedlings (Figure 4, A, B, G, and H, green curves). For technical reasons, resuming roGFP2 measurements after intermittent illumination of seedlings outside the plate reader was only possible after a lag time of about 10 s post-illumination, since the plates needed to be transferred back into the reader. Conversely, the sensors in the cytosol in control plants did not respond to illumination alone (Figure 4, D and E, green lines). The combination of MV and illumination, however, induced an increase in the fluorescence ratio for both sensors in all three compartments,

resulting in a transitory peak of oxidation lasting close to 10 min after illumination. The long-term measurement shows a gradual oxidation over time (Figure 4). This oxidation was dependent on the concentration of MV applied, albeit with different amplitudes depending on the probe and on the compartment. While Grx1-roGFP2 in the cytosol showed a pronounced long-term ratio increase in plants pre-incubated with 50 and $100 \mu\text{M}$ MV, the ratio change of cytosolic roGFP2-Orp1 was limited to a minor reversible increase only (Figure 4, D–F). In mitochondria, light exposure caused transient oxidation of roGFP2-Orp1 and roGFP2-Grx1 albeit without pronounced differences between the two probes (Figure 4, G–I). The current plate reader set up did not allow to resolve sensor dynamics during light exposure; instead measurements had to be carried out after light exposure. This limitation accounts in more general to fluorescent biosensing in response to light and was only recently overcome using a custom imaging setup that can only be used at lower throughput (Elsässer et al., 2020). However, immediately after restarting the recording following an intermittent 1-h illumination period a rapid decrease of the fluorescence ratio from a transient oxidation peak was observed. This decline is visible in mitochondria and most pronounced in the cytosol. The rapid decrease in the fluorescence ratios hints at a far more pronounced transient oxidation during the illumination period.

Chloroplasts and mitochondria contribute to MV-induced oxidative stress

Flash illumination for roGFP2 fluorescence measurements during plate reader-based fluorescence excitation with intervals of 1 h did not lead to changes in roGFP2 fluorescence ratios in chloroplasts and the cytosol (Supplemental Figure S6B). In mitochondria, however, the fluorescence ratio did show a small increase pointing at the possibility of an autonomous mitochondrial oxidative response, which was also recently concluded by independent work using orthogonal approaches (Cui et al., 2019). To dissect the relative contributions of chloroplasts and mitochondria to the MV-induced oxidative response in the cytosol, we used inhibitors for both ETCs. Seedlings expressing the different sensors were immersed in medium containing either $10 \mu\text{M}$ 3-(3,4-dichlorophenyl)-1,1-dimethylurea (DCMU) to inhibit the electron transport between PSII and plastoquinone, or $50 \mu\text{M}$ rotenone to inhibit the mETC at complex I (Figure 5, A and B). The presence of DCMU decreased MV-induced oxidation of both plastid-targeted sensors compared to seedlings treated with MV alone (Figure 5, C and F, green and black curves). The inhibitory effect of DCMU was most evident immediately after illumination in seedlings expressing Grx1-roGFP2. In seedlings expressing roGFP2-Orp1, DCMU also inhibited the oxidation of the sensor, albeit to a lesser extent. Inhibition of the pETC by DCMU also completely abolished the light-induced oxidation of cytosolic Grx1-roGFP2 and roGFP2-Orp1 (Figure 5, D and G) and mitochondrial roGFP2-Grx1 (Figure 5E). At the same time,

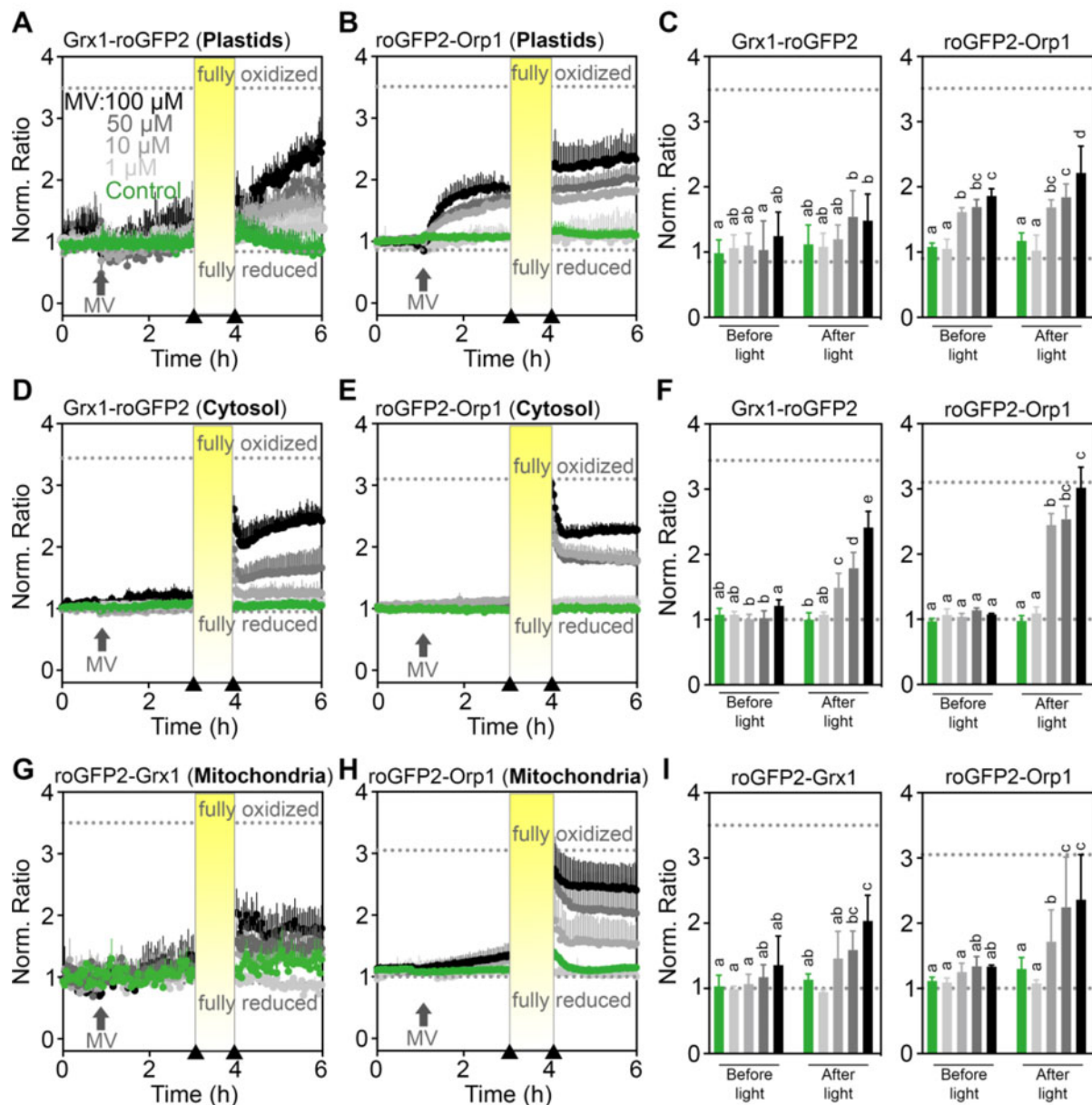


Figure 4 Light enhances MV-induced oxidation of roGFP2-derived redox sensors. A–I, Seven-day-old seedlings stably expressing the indicated sensor constructs in plastids, in the cytosol or in mitochondria were placed in a 96-well plate with imaging buffer. After 1 h, MV was added to final concentrations as indicated in (A). Arrows on the x-axes of (A, B, D, E, G, and H) indicate the time points at which data for the bar charts in (C, F, and I) were extracted (i.e. before and after illumination). In control samples (green), only buffer was added. Oxidation of the sensors was recorded as the normalized ratio of the fluorescence recorded with excitation at 410 ± 5 nm and 480 ± 5 nm, respectively. Fluorescence was always recorded at 530 ± 20 nm. After a pre-incubation with MV for 2 h, seedlings were intermittently illuminated for 1 h with actinic light ($200 \mu\text{mol m}^{-2} \text{s}^{-1}$) and redox measurements were subsequently resumed for 2 h. Dotted lines indicate ratio values measured from the same wells at the end of the experiment after incubation in 20 mM DTT for full reduction or 100 mM H₂O₂ for full oxidation of the probes. Mean ratios + SD, $n \geq 4$ biological replicates, where each replicate is an independent pool of 4–5 seedlings. Different letters represent statistical differences between ratios after log₁₀ transformation, according to one-way ANOVA with Tukey's multiple comparison test ($P < 0.05$). Data for individual channels can be found in Supplemental Figure S8.

DCMU also partially abolished the fluorescence ratio increase of mitochondrial roGFP2-Orp1 to about 50%–70% of ratio values in control seedlings (Figure 5H); 50 μM rotenone partially suppressed the ratio increase of Grx1-roGFP2 in chloroplasts and cytosol induced by the combination of MV and light (Figure 5, C and D, dark red and black curves).

The inhibitory effect of rotenone, however, was less pronounced than the inhibition caused by DCMU and did not affect the decline in fluorescence ratios of both sensors seen immediately after restart of the measurements following the illumination period (Figure 5, C and D). In contrast to Grx1-roGFP2, roGFP2-Orp1 fluorescence in plastids and the

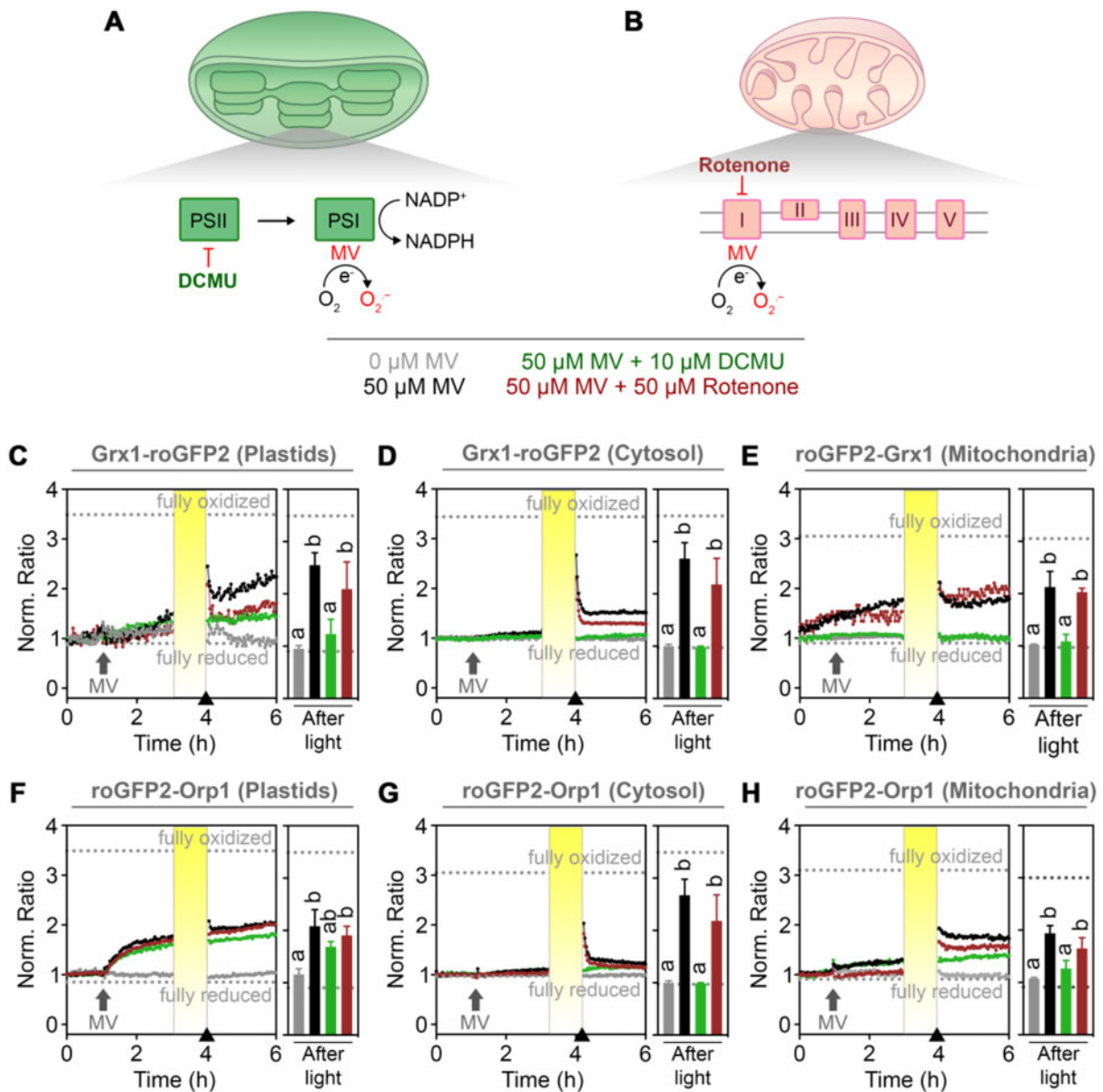


Figure 5 Contribution of chloroplast and mitochondrial ETCs to MV-induced oxidation. A, Model depicting the function and interplay of MV and ETC inhibitors on superoxide production in a chloroplast. MV withdraws electrons (e^-) from PSI and transfers them to molecular oxygen (O_2) to form superoxide ($O_2^{\cdot-}$). DCMU is an inhibitor that specifically blocks electron transfer from PSII to plastoquinone. B, In the mitochondrion, MV is able to transfer electrons from complex I of the mitochondrial ETC to O_2 , generating $O_2^{\cdot-}$. Rotenone inhibits complex I activity. C–H, Seven-day-old seedlings stably expressing the indicated sensor constructs in plastids, cytosol or mitochondria were placed in 96-well plates with imaging buffer as a control or buffer supplemented with 10 μ M DCMU or 50 μ M rotenone to inhibit the electron flux along the chloroplastic or mitochondrial ETCs, respectively. After 1 h, MV was added to a final concentration of 50 μ M or buffer as a control. After 2 h of treatments, the samples were intermittently exposed to 1 h of actinic light (200 μ mol $m^{-2} s^{-1}$). Data indicate the mean normalized ratio of the sensor fluorescence sequentially excited at 410 ± 5 nm and 480 ± 5 nm, and collected at 530 ± 20 nm in at least four biological replicates (left panels). Arrows on the x-axes of (C–H) indicate the time point at which data for the bar charts (right panels). Dotted lines indicate ratio values measured from the same wells at the end of the experiment during incubation in 20 mM DTT for full reduction or 100 mM H_2O_2 for full oxidation of the probes. Different letters represent statistical differences between ratios after \log_{10} transformation, according to one-way ANOVA with Tukey's multiple comparison test ($P < 0.05$).

cytosol was not altered by rotenone (Figure 5, F and G). In mitochondria, rotenone caused a slight suppression of the ratio increase of roGFP2-Grx1 and roGFP2-Orp1 during the time between addition of MV and illumination of seedlings 2 h later. After the illumination period, slightly lower ratio

values compared to control seedlings were found for roGFP2-Orp1 in mitochondria although the dynamics with a decrease after the illumination were not affected (Figure 5H). This confirms that the pETC provides a major contribution to the light-induced oxidation in all three

compartments, while the mETC contributes to a lesser extent at illumination.

Discussion

Dynamic recording of oxidative processes in multiple subcellular compartments of plant tissues using plate reader-based fluorimetry

Redox-sensitive GFPs have paved the way to elucidate the distinct differences in local E_{GSH} of subcellular compartments in plant cells (Jiang et al., 2006; Meyer et al., 2007; Schwarzländer et al., 2008). While roGFP2-based sensors for E_{GSH} are highly robust and reliable, sensor constructs for H_2O_2 monitoring are more diverse exhibiting different strength and limitations (Schwarzländer et al., 2016). Probe variants of the HyPer family have been used multiple times in different subcellular compartments (Costa et al., 2010; Boisson-Dernier et al., 2013; Exposito-Rodriguez et al., 2017; Rodrigues et al., 2017; Mangano et al., 2018). Because HyPer is based on a circular permuted YFP a cleft in the artificial barrel structure allows direct access of protons to the central chromophore rendering most HyPer probes highly sensitive to pH, a feature that could potentially cause major artefacts in light-dependent measurements in chloroplasts (Belousov et al., 2006; Schwarzländer et al., 2014). An updated version, HyPer7, has been proven to be pH-insensitive, but has not yet been used in plant research (Pak et al., 2020). Fusions of roGFP2 with peroxidases like the GPX Orp1 or PRXs, such as Tsa2 overcome this limitation because the roGFP2 ratio is pH-insensitive over the whole physiological range (Schwarzländer et al., 2008; Gutscher et al., 2009; Morgan et al., 2016). Orp1 fused to roGFP2 was chosen in this work based on its sensitivity to low H_2O_2 levels (Delaunay et al., 2002; Sobotta et al., 2013), its pH-insensitivity, and its dependence on reduction via Grx and GSH (Nietzel et al., 2019).

Environmental stress conditions can trigger oxidative processes via ROS formation. However, oxidation occurs with different dynamics and amplitudes in different subcellular compartments (Schwarzländer et al., 2009; Rosenwasser et al., 2011; Bratt et al., 2016). Dynamic measurements after triggering oxidative stress have been successfully carried out in the cytosol and mitochondria of cells and tissues placed in perfusion chambers on fluorescence microscopes (Schwarzländer et al., 2009). While high-throughput approaches are limited in a typical microscopy set-up, plate reader-based approaches have enabled dynamic long-term measurements with multiple parallel samples in one experiment (Rosenwasser et al., 2010, 2011; Bratt et al., 2016; Nietzel et al., 2019; Wagner et al., 2019). Comparative measurements with Grx1-fused roGFP2 for E_{GSH} and roGFP2-Orp1 for H_2O_2 sensing recently revealed differential responses of both probes in the cytosol and the mitochondrial matrix (Nietzel et al., 2019). Our results show that this approach can be extended to the chloroplasts, as the predominant generators of ROS under illumination (Mubarakshina et al., 2010).

While genetically encoded biosensors can be powerful tools for in vivo monitoring of physiological parameters, potential problems caused by overexpression, mis-targeting or incomplete targeting have been observed (Albrecht et al., 2014; De Col et al., 2017). In contrast to a slight developmental delay that we observed previously for Arabidopsis plants with mitochondrial roGFP2-Orp1 (Nietzel et al., 2019), Grx1-roGFP2 and roGFP2-Orp1 can both be targeted to plastids without any mis-targeting and without causing any apparent developmental phenotype. The absence of obvious phenotypes suggests that the reporter constructs and their import do not interfere with normal plastid functions. In microscopic experiments with high spatial resolution, incomplete targeting may not pose a major problem or can even be exploited as an advantageous feature for simultaneous recording of physiological responses in two compartments (Marty et al., 2019). As we employ plate reader assays in which only the overall fluorescence from a biological sample is recorded, correct targeting of the probes to all compartments is of utmost importance and was carefully validated.

Previous reports using roGFP-based sensors have demonstrated a fast and reversible oxidation in response to external H_2O_2 (Meyer et al., 2007; Morgan et al., 2011). We observed similar fast oxidation kinetics for both tested sensors in the cytosol of Arabidopsis seedlings; 8–10 mM H_2O_2 were sufficient to reach the maximum oxidation of the sensors. This maximum oxidation, however, was not maintained but rather followed by an immediate recovery toward the fully reduced state over the course of 5 h in WT plants. This decrease in the fluorescence ratios of roGFP2 after severe oxidative challenge indicates a decrease of intracellular H_2O_2 and re-reduction of the cytosolic glutathione buffer, respectively. This recovery shows the remarkable efficiency of the plant peroxide detoxification machinery, enabling 4–5 seedlings with a total fresh weight of ~15 mg to clear a total volume of 200 μL from 10 mM H_2O_2 within 5 h. This would amount to an average detoxification of about 440 nmol (g FW)⁻¹ min⁻¹, which interestingly is in the order of 50–5,000 nmol (g FW)⁻¹ that has been reported for the H_2O_2 content in unstressed leaves (Queval et al., 2008).

The severely delayed or even completely abolished decline in fluorescence ratios after addition of H_2O_2 in *cat2* mutants, highlights the importance of peroxisomal CAT2 for degradation of external H_2O_2 entering the cytosol. Catalase 2 is the predominant catalase isoform in Arabidopsis and needed to control H_2O_2 in the light (Mhamdi et al., 2010). The sensor-based approaches do not allow for quantification of H_2O_2 (Schwarzländer et al., 2016; Nietzel et al., 2019). Based on the in vitro sensitivities of the two sensor proteins, it can be considered that with steady-state concentrations of H_2O_2 in the low micromolar range in the cytosol both sensors would be completely oxidized. The observed fast oxidation kinetics together with the catalase-dependent recovery of the fluorescence ratio support the view that H_2O_2 can readily pass both plasma membrane and the

peroxisomal membrane at sufficient rates to achieve and maintain this oxidation. Although not investigated in more detail here, it has to be assumed that aquaporins provide the apparent permeability of the membranes for H_2O_2 (Bienert and Chaumont, 2014; Rodrigues et al., 2017). While CAT2 clearly affects the recovery, it does not impact the initial oxidation achieved with different amounts of external H_2O_2 . This implies that the initial oxidation of probes is limited by the uptake rate of H_2O_2 into the cells and that concentrations of about 10 mM H_2O_2 are necessary to drive the roGFP2 probes into full oxidation. The transitory peak for the maximum oxidation emphasizes the need for immediate measurement of complete sensor oxidation for calibration purposes or the use of even higher concentrations of external H_2O_2 to achieve complete and sustained in situ oxidation of roGFPs (Schwarzländer et al., 2008; Marty et al., 2009). Taken together, the experimental setup optimized here will be well suited for further genetic dissection of cellular peroxide detoxification systems (Smirnov and Arnaud, 2019).

Real-time monitoring of MV-induced oxidative stress

Plants frequently contain a broad range of autofluorescent endogenous compounds (Müller et al., 2013). Reliable interpretation of sensor responses thus depends on correct recording and subtraction of such signals underlying and potentially obscuring the true roGFP2 signal (Fricker, 2016). While for short-term treatments with oxidative changes induced by light and/or MV this can be done reliably and additionally controlled for by careful monitoring the raw data for each individual channel, deviations in long-term measurements cannot be fully excluded. For long-term recordings, we found that in some cases MV treatment led to strong changes of the apparent ratio recorded for both roGFP2-based probes in vivo even though the individual channels showed little change. Although we cannot fully explain the exact kinetics of the fluorescence ratio recorded over several hours after MV treatment, we show that the reported effects of MV and light are reliable and reproducible. In addition, inhibitor treatments confirmed that the observed effects are causally connected to primary oxidation occurring in the respective subcellular compartments.

From tracer studies, it is known that MV-uptake reaches saturation after 2 h (Fujita et al., 2012; Xi et al., 2012). Therefore, we chose 2 h of MV incubation prior to light treatment. During this time, ROS formation caused by MV is limited either by uptake of MV or by light exposure to drive electron transport in the pETC. Even without additional illumination of seedlings, MV caused oxidation in chloroplasts, and to a minor extent in mitochondria and the cytosol. This contrasts with earlier measurements in which MV caused a minor oxidation in mitochondria and a pronounced oxidation in the cytosol of Arabidopsis cotyledons (Schwarzländer et al., 2009). A major difference between the two experiments is the use of a confocal microscope with

laser excitation targeting a small number of cells by (Schwarzländer et al., 2009), while a plate reader with less intense excitation light collecting fluorescence from whole seedlings was used in this work. In the first 2 h after MV addition, the response of the roGFP2-Orp1 sensor was faster and more pronounced compared to Grx1-roGFP2 in plastids or roGFP2-Grx1 in mitochondria, which indicates an increase of H_2O_2 before a change in E_{GSH} . However, because the oxidized roGFP2-Orp1 depends on GSH for its reduction and because the roGFP2 domain may on its own react with GSH/GSSG, a gradual change in sensor oxidation may also reflect changes in the E_{GSH} . If both sensors react to imposed stress (i.e. 5 h after MV addition), it is thus not possible to dissect whether the observed oxidation is caused by H_2O_2 production or an increase of E_{GSH} (Meyer and Dick, 2010; Nietzel et al., 2019). We observed complete oxidation of plastid-targeted roGFP2-Orp1 and partial oxidation of plastid-targeted Grx1-roGFP2 after MV addition, indicating that the excitation light in the plate reader is still sufficient to trigger electron flux in the pETC and hence the formation of ROS (Supplemental Figure S6). The MV-induced oxidation was considerably slower than the oxidation induced by incubation of seedlings in H_2O_2 (Figure 3), in accordance with only intermittent illumination during plate reader measurements. Although it is not possible to quantify the absolute amount of H_2O_2 produced in plastids during the MV challenge, it is plausible to hypothesize that the amount of H_2O_2 reaching the cytosol is far below concentrations reached when millimolar H_2O_2 concentrations were added externally. The minor oxidation observed for cytosolic sensors after MV challenge indicates that either low amounts of ROS are leaving the chloroplasts under these conditions, or that the capacity of the cytosolic scavenging systems is sufficient to detoxify the H_2O_2 leaking from chloroplasts. H_2O_2 produced in chloroplasts may be detoxified locally through the ascorbate-glutathione cycle. The E_{GSH} in each compartment is independent and not directly correlated (Marty et al., 2019). The resultant GSSG is contained within the organelles, leading to a local change in E_{GSH} to less reducing values. The lethal phenotypes of Arabidopsis mutants deficient in plastidic GR2 strongly suggest that GSSG cannot be efficiently exported from plastids (Marty et al., 2019). In addition, stromal E_{GSH} responds dynamically to light (Haber and Rosenwasser, 2020; Müller-Schüssele et al., 2020) and GSSG can be formed via several enzymes directly or indirectly involved in ROS scavenging (DHAR, GRX, PrxII, MSR1, among others), and is efficiently recycled by GR2.

ROS as a putative mobile signal between cellular sub-compartments

In photosynthetic organisms, light exposure triggers activation or inactivation of multiple redox-regulated enzymes containing thiol-switches (Cejudo et al., 2019). From high light treatments of plants transiently expressing HyPer, it was deduced that oxidation in plastids and the nucleus takes less than one second (Exposito-Rodriguez et al., 2017).

In our experiments, we show a change in the oxidation of sensors targeted to plastids and mitochondria in plants exposed to light (Figure 4, A, B, G, and H, green curves), indicating that light exposition changes the redox homeostasis in these compartments. Further research will be needed to increase the time resolution of these light-induced redox changes, especially using pH-insensitive sensors such as roGFP2-Orp1 and Grx1-roGFP2, since pH adjustments may be challenging for fast events.

Light exposure of samples pretreated with MV increased the oxidation in chloroplasts, cytosol, and mitochondria more than MV alone (Figure 4), in accordance with enhanced MV toxicity due to pETC activation (Cui et al., 2019). Oxidation of the Grx1-roGFP2 and roGFP2-Grx1 in all compartments was dependent on the pETC, as it was inhibited by DCMU. This was the same for roGFP2-Orp1 targeted to cytosol and mitochondria, while only a minor inhibition was observed in plastids (Figure 5, F–H). This may indicate that the concentration of DCMU used still allows H_2O_2 production in the chloroplast or that it enhances the production of peroxides through production of singlet oxygen (Fufezan et al., 2002; Krieger-Liszkay, 2005; Dietz et al., 2016). In this same sensor line, no oxidation peak was observed immediately after light exposure (Figure 4). This peak might have been missed due to a slightly slower transfer of the well plate back into the plate reader.

Our data clearly show that an oxidative challenge in chloroplasts that shifts both, H_2O_2 flux as well as stromal E_{GSH} , entails a dynamic change in cytosolic as well as mitochondrial E_{GSH} and H_2O_2 flux (Figure 5, C–H). A transient oxidation peak apparent in the cytosol immediately after an extended illumination period and a more long-term change in E_{GSH} and H_2O_2 reveals the extent of this redox-linkage between the compartments. It is likely that ROS produced in the chloroplast can evade the local scavenging system and affects redox homeostasis in the cytosol and mitochondria by direct membrane passage. We cannot exclude secondary effects, however, such as signaling-mediated changes in subcellular antioxidant capacities, contributing to the responses of E_{GSH} and H_2O_2 flux in the different compartments.

In mammals and other nonphotosynthetic organisms, mitochondria constitute the main source of ROS production under MV treatments (Cochemé and Murphy, 2008). Our findings showed mild oxidation in the mitochondrial matrix after addition of MV (Figure 3, G–I), which can also be observed in the fluorescence intensity shifts of both individual channels at the moment of MV addition to seedlings expressing the mitochondria-targeted roGFP2-Orp1 (Supplemental Figures S4F and S8F). This initial oxidative shift even before the light treatment was inhibited in plants pretreated with the mETC inhibitor rotenone but not with the pETC inhibitor DCMU (Figure 5H). This indicates that MV toxicity in mitochondria is independent from the chloroplastic pETC. Notably, rotenone also slightly lessened the oxidation of Grx1-roGFP2 in plastids and the cytosol in

response to light/MV (Figure 5, C and D), suggesting either an effect of rotenone on pETC or interdependence of mETC and pETC. In isolated barley thylakoids, rotenone inhibits a NAD(P)H dehydrogenase-like enzyme (NDH), which is implicated in cyclic electron transport via photosynthetic complex I (Teicher and Scheller, 1998). Despite its original name, NDH has been recently shown to preferentially accept electrons from ferredoxin rather than NADPH (Schuller et al., 2019). The key role of NDH in cyclic electron transport may nevertheless explain a direct modulation of light-induced MV toxicity by rotenone. In addition, mitochondria and chloroplasts are metabolically coupled (Schöttler and Tóth, 2014; Shameer et al., 2019). Therefore, we cannot discard an indirect inhibition of the pETC by decreasing the mETC with rotenone. Indeed, we have recently confirmed such a link via the malate valves (Elsässer et al., 2020), which would suggest an increase in NADPH availability in the plastid stroma at inhibited mitochondrial respiration. Whether that leads to stronger glutathione reduction, or rather oxidation through photoinhibition-derived ROS production is unclear, but our data suggest the former.

Efficient inhibition of the mETC with rotenone and the pETC with DCMU led to concomitant abolishment of MV-induced changes in both sensors. This observation further supports the notion that the responses of both probes are causally connected to the activity of either ETCs. The interpretation of alterations in roGFP2 fluorescence as a measure of oxidative responses linked to deviations of electrons from the ETCs thus appears valid (Figure 6). Similarly, the presented data show that inhibitor-dependent abolishment of oxidation in the cytosol caused by MV in conjunction with light strongly suggests linkage between the redox response in chloroplasts and cytosol (Figure 5). With the respective probes and the plate reader setup, it is thus possible to measure the immediate and dynamic oxidative response to a stress imposed on chloroplast, in the cytosol and mitochondria. Pulsed short-term stresses like e.g. short periods of strong illumination are followed by a recovery phase. Only if the stress occurs at higher frequencies or even persists permanently, this results in a long-term oxidation.

While both roGFP2-based probes used here show an oxidative response after MV treatment within hours, it is already known that exposure of plants to MV triggers distinct changes in gene expression. In cucumber, MV causes the accumulation of ROS and lipid peroxides after 1 h, while GSH oxidation and an increase in APX and GPX activities were identified 48 h after MV application (Liu et al., 2009). Light acts as an enhancer of the MV-induced oxidation, but is not essential for MV-induced oxidative damage (Cui et al., 2019; Shapiguzov et al., 2019).

The exact mechanisms by which different redox pools in different compartments interact and orchestrate signaling remain largely unclear. Under high-light stress, the association between plastids and the nucleus increases (Exposito-Rodriguez et al., 2017), potentially fostering a direct transfer of ROS from the plastids to the nucleus.

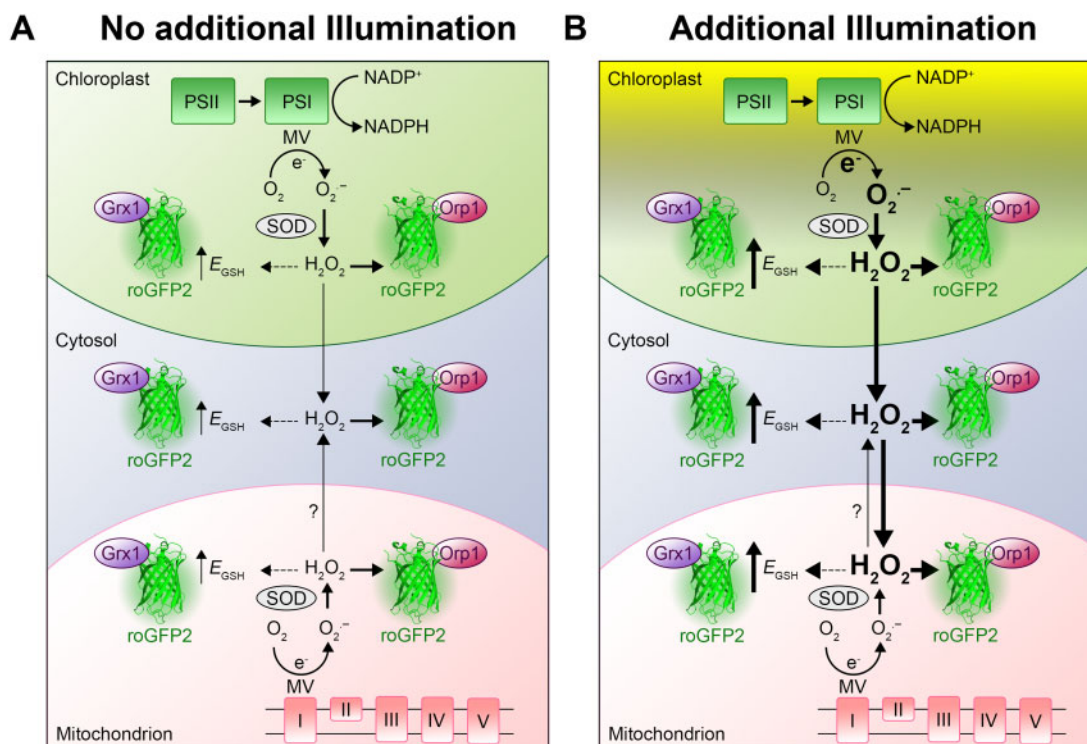


Figure 6 Increased chloroplast-derived ROS production caused by MV modulates the E_{GSH} in chloroplasts, cytosol, and mitochondria. A, MV is an herbicide that causes photo-oxidative stress in chloroplasts by diverting electrons from the PSI to molecular oxygen (O_2), leading to formation of superoxide ($O_2^{\cdot -}$). In addition, MV is able to transfer electrons from complex I of the mitochondrial ETC to O_2 , also generating $O_2^{\cdot -}$. Superoxide is dismutated to H_2O_2 by chloroplastic or mitochondrial SODs. Increased accumulation of H_2O_2 can lead to oxidation of the glutathione buffer, most likely via detoxification along the ascorbate–glutathione cycle (data not shown). B, Additional light enhances electron transport in the chloroplasts, inducing the production of $O_2^{\cdot -}$ and in consequence also H_2O_2 . If the scavenging capacities of the chloroplast are surpassed, H_2O_2 might be leaking to the cytosol and mitochondria. H_2O_2 can indirectly increase local E_{GSH} , which can be tracked using Grx1-roGFP2. The increase of H_2O_2 can be tracked using the oxidation of the roGFP2-Orp1 sensor.

Chloroplastic H_2O_2 is believed to act as a secondary messenger involved in retrograde signaling to the nucleus (Chan et al., 2016), where it can modulate gene expression as measured at the transcript level (Sewelam et al., 2014). As an example, the over-excitation of PSI can lead to ROS-induced changes in the redox state of antioxidant-related transcription factors such as ZAT10 (Rossel et al., 2007) and HSFA1D, the latter can enhance the expression of the peroxidase APX2 (Jung et al., 2013). It is possible that the transfer of ROS from plastids to the cytosol might be facilitated by aquaporins (Mubarakshina et al., 2010). In mammals, Aqp8 and Aqp11 have been already characterized as essential ROS transporters from mitochondria and the endoplasmic reticulum, respectively (Chauvigné et al., 2015; Bestetti et al., 2020). In tobacco (*Nicotiana tabacum*) chloroplasts, the aquaporin NtAQP1 has been described as a gas pore for CO_2 (Uehlein et al., 2008), while plant mitochondria harbor at least one aquaporin, TTIP5; 1, which is still uncharacterized (Bienert and Chaumont, 2014). Dynamic recordings of ROS formed by the chloroplastic and mitochondrial ETCs and downstream oxidative changes in other subcellular compartments as established in this work present opportunities for future research regarding the mechanisms involved in the mobility of ROS across (intra-)cellular membranes.

Conclusions

In this work, we have established a simple semi high-throughput approach to follow the contribution of different subcellular compartments to a ROS-mediated oxidation response in living tissues for multiple seedlings and treatment regimes in parallel. The results identify chloroplasts as the principal source of ROS in response to MV in illuminated, photosynthetically active tissue but also highlight the contribution of mitochondria to MV toxicity within plant cells. The ability to record dynamic redox-related changes will pave the way to better understand the interplay between redox imbalances in distinct plant compartments. In future experiments, measuring coupled redox dynamics in combination with genetics will enable further dissection of the signaling events between subcellular compartments.

Materials and methods

Plant material and growth conditions

Arabidopsis (*Arabidopsis thaliana*) Col-0 ([L.] Heynh.) plants were obtained from the Nottingham Arabidopsis Stock Centre (www.arabidopsis.info). Col-0 expressing the Grx1-roGFP2 sensor in either the cytosol or the plastids, or roGFP2-Grx1 in mitochondria have been described earlier

(Marty et al., 2009, 2019; Speiser et al., 2018). Cytosolic and mitochondrial targeted versions of roGFP2-Orp1 in Col-0 as well as in CAT2-deficient, *cat2* (SALK_076998) were previously reported (Nietzel et al., 2019). For experiments with whole seedlings, seeds were surface-sterilized with 70% (v/v) ethanol, rinsed three times with sterile deionized water and stratified for 48 h at 4°C. Seeds were then sown on plates with 0.5 × Murashige and Skoog (MS) growth medium (Murashige and Skoog, 1962; Duchefa Biochemie, Haarlem, The Netherlands) supplemented with 0.1% (w/v) sucrose, 0.05% (w/v) MES (pH 5.8, KOH) and 0.8% (w/v) agar. Plates were incubated vertically in a growth chamber under a long-day regime (16 h light, 22 ± 2°C; 8 h dark 18 ± 2°C) with a photon flux density of 100 μmol m⁻² s⁻¹ for 7 d.

Cloning of plastid-targeted roGFP2-Orp1 sensor and generation of transgenic plant lines

The roGFP2-Orp1 sequence was amplified by PCR from pBSSK:roGFP2-Orp1 (Gutscher et al., 2009) and fused to the target peptide of transketolase (TK_{TP}) analogous to the mitochondrial sensor constructs described in (Nietzel et al., 2019). Primers for roGFP2-Orp1 amplification were AACCA TAGAGAAACTGAGACTGCGGTGAGCAAGGGCGAGGAG CTGTTC and GTACAAGAAAGCTGGGTCTATTCCACCT CTTTCAAAGTTCTTC and for amplification of the targeting peptide TACAAAAAAGCAGGCTTCACCATGGCGTCTT CTTCTTCTCTCACT and GAACAGCTCCTCGCCCTTGCTC ACCGCAGTCTCAGTTTTCTCTATGGTT. Fusion of both constructs was achieved by amplification with the primers GGGGACAAGTTTGTACAAAAAGCAGGCTTCACC and GGGGACCACTTTGTACAAGAAAGCTGGGTCTA. For constitutive plant expression (CaMV 35S promoter), the amplicon was cloned into pDONR207 (Invitrogen Ltd, Carlsbad, CA, USA) and then into pH2GW7 (Karimi et al., 2002) using Gateway cloning (Invitrogen Ltd, Carlsbad, CA, USA). For the generation of a *cat2* reporter line with expression of Grx1-roGFP2 in the cytosol, plants were transformed with the plasmid pBinAR-Grx1-roGFP2 described previously (Marty et al., 2009). Transformed seeds were selected in 50 μg mL⁻¹ kanamycin, screened for fluorescence, and segregated until homozygous lines were obtained.

Validation of subcellular roGFP2 targeting by confocal microscopy

Seven-day-old seedlings were imaged using a confocal laser scanning microscope (Zeiss LSM 780, connected to an Axio Observer.Z1; Carl Zeiss Microscopy, Jena, Germany) with a 63 × lens (Plan-Apochromat 63 × /1.4 Oil DIC M27). GFP and chlorophyll fluorescence were measured by excitation at 488 nm (Argon laser, power output: 1%, detector gain: 665) and emission at 505–530 nm (GFP) and 650–695 nm (chlorophyll). For mitochondrial counter staining, seedlings were vacuum infiltrated for 30 min with 200 nM MitoTracker Orange (Thermo Fisher Scientific, Waltham, MA, USA) and measured by excitation at 543 nm (Helium-Neon

(HeNe) laser, power output: 12%, detector gain: 754) and emission at 570–623 nm.

Purification of recombinant roGFP2 variants

Escherichia coli HMS174/Origami cells containing the pET30-roGFP2-His vector were cultured in liquid LB medium supplemented with 50 μg mL⁻¹ kanamycin at 37°C to an OD₆₀₀ of 0.6–0.8. roGFP2-His expression and cell lysis were performed as described in (Nietzel et al., 2019). The lysate was centrifuged at 19,000g for 15 min at 4°C and the supernatant filtered through a sterile filter of 0.45 μm nominal pore size. The filtered fraction was then loaded onto a Ni-NTA HisTrapTM column (GE Healthcare, Little Chalfont, UK) using a peristaltic pump at a flow rate of 1 mL min⁻¹. Proteins were eluted from the column with a 10–200 mM imidazole gradient (100 mM Tris-HCl, pH 8.0, 200 mM NaCl) using an ÄKTA Prime Plus chromatography system (GE Healthcare). Fractions were collected and stored at 4°C.

Spectral measurement of roGFP2 probe variants in planta

Pools of 7-d-old seedlings (4–5 seedlings per pool) were placed in 200 μL imaging buffer (10 mM MES, 10 mM MgCl₂, 10 mM CaCl₂, 5 mM KCl, pH 5.8) in transparent Nunc[®] 96-well plates. Samples were excited at 370–496 nm with a step width of 1 nm and the emission collected at 530 ± 5 nm using a CLARIOstar plate reader (BMG Labtech, Offenburg, Germany). To achieve complete reduction or oxidation of the sensor, the imaging buffer was supplemented with either 20 mM DTT or 100 mM H₂O₂. Nontransformed WT seedlings were treated in the same conditions and used to determine the autofluorescence that was subtracted from the fluorescence recorded in roGFP2 lines. The spectral properties of recombinant roGFP2 were measured under the same conditions.

Time-resolved ratiometric analysis of probe fluorescence in planta

All in planta measurements for all different probes were conducted in pools of 7-d-old seedlings submerged in imaging buffer using either a CLARIOstar or POLARstar plate reader (BMG Labtech) following step-by-step protocols outlined in (Ugalde et al., 2020a). roGFP2 was excited by a filter-based excitation system at 410 ± 5 nm and 480 ± 5 nm. Fluorescence was collected using either a 530 ± 20 filter for the POLARstar, or a 520 ± 5 nm for the CLARIOstar. Orbital averaging based on 26 flashes along a circle of 3 mm diameter within each well was used to account for heterogeneous distribution of tissue across the wells. The fluorescence ratio was calculated as 410 nm/480 nm and normalized to the ratio value at the start of them experiment (*t* = 0 h). Different amounts of H₂O₂ were added to each well using the built-in automated injectors to reach different concentrations of H₂O₂ in a final volume of 200 μL. To induce oxidative stress in seedlings by endogenous ROS production, 20 μL of MV (Sigma-Aldrich, Steinheim, Germany) from stock solutions of different concentrations were manually added to each well

to reach the required final concentrations. Two hours after start of the incubation of seedlings in MV-containing buffer, actinic light treatments were performed by exposing the seedlings in the plate to white LED light with a photon flux density of $200 \mu\text{mol m}^{-2} \text{s}^{-1}$ for 1 h. Subsequently, the recording of roGFP2 fluorescence was continued in the dark (except for the short light flashes required for the measurements) within the plate reader. To assess the dynamic range of the probes in planta and for sensor calibration, 20 mM DTT and subsequently 100 mM H_2O_2 were added at the end of each experiment to fully reduce and fully oxidize the sensors. Between these treatments, samples were rinsed twice with imaging buffer. In each experiment, at least four technical replicates consisting of 4–5 pooled seedlings per well were used. Each experiment was repeated at least three times.

Samples were incubated with inhibitors of chloroplast and mitochondrial ETC prior to the addition of MV. To inhibit PSII, samples were treated with 10 μM DCMU dissolved in ethanol, whereas 50 μM rotenone (Sigma-Aldrich) was dissolved in dimethyl sulfoxide to inhibit complex I of the ETC in mitochondria.

Estimating of changes in ROS production by chemical probing

Seven-day-old seedlings were floated for 4 h on imaging buffer as a control or on imaging buffer supplemented with 100 μM MV and incubated under actinic light to induce photo-oxidative stress. Seedlings were then transferred to a staining solution of 25 μM $\text{H}_2\text{DCF-DA}$ (Sigma-Aldrich) in 10 mM Tris-HCl (pH 7.4) and incubated in the dark for 30 min. The seedlings were washed three times with 10 mM Tris Buffer (pH 7.4) and imaged using a confocal laser scanning microscope with a $5\times$ (EC-Plan-Neofluar $5\times/0.16 \text{ M27}$) lens. DCF fluorescence was recorded at 505–530 nm after excitation at 488 nm. Fluorescence was quantified as intensity per μm^2 of leaf tissue using Fiji (Schindelin et al., 2012) and expressed as arbitrary units (AUs) per μm^2 .

Statistical analyses

For analyses of fluorescence ratio data statistical differences were calculated between ratios after \log_{10} transformation, according to one-way ANOVA with Tukey's multiple comparison test ($P < 0.05$).

Accession numbers

Sequence data for the gene coding for catalase 2 can be found in the GenBank/EMBL data libraries under accession number AT4G35090 (CAT2).

Funding

This work was supported by the Deutsche Forschungsgemeinschaft (DFG) through the Research Training Group GRK 2064 'Water use efficiency and drought stress responses: From Arabidopsis to Barley' (A.J.M.; M.S.; S.J.M.-S.; U.C.V.), grants ME1567/9-1/2 and SCHW719/7-1 within the Priority Program SPP1710 "Dynamics of thiol-based redox

switches in cellular physiology" (A.J.M.; M.S.), the MSC-ITN project no. 607607 "CALIPSO" (U.C.V.; E.A.C.), grant MU 4137/1-1 (S.J.M.-S.), and the Emmy-Noether programme (SCHW719/1-1; M.S.).

Conflict of interest statement. None declared.

Supplemental data

Supplemental Figure S1. Subcellular localization of roGFP2-based probes for the glutathione redox potential (E_{GSH}) and hydrogen peroxide (H_2O_2) in Arabidopsis.

Supplemental Figure S2. Raw fluorescence of Arabidopsis E_{GSH} and H_2O_2 sensors lines compared with non-transformed Col-0 plants.

Supplemental Figure S3. Calibration procedure to determine the dynamic range of the sensor exemplified for cytosolic roGFP2-Orp1.

Supplemental Figure S4. Individual excitation channels of roGFP2 fluorescence upon MV-induced oxidation in planta.

Supplemental Figure S5. MV treatment causes massive ROS production in leaves.

Supplemental Figure S6. Effect of the excitation light on the MV-induced oxidation of the roGFP2-Orp1 sensor.

Supplemental Figure S7. Effect of extended treatment of Arabidopsis seedlings with MV.

Supplemental Figure S8. Individual excitation channels of roGFP2 fluorescence upon light-enhanced MV-induced oxidation in planta.

References

- Albrecht SC, Sobotta MC, Bausewein D, Aller I, Hell R, Dick TP, Meyer AJ (2014) Redesign of genetically encoded biosensors for monitoring mitochondrial redox status in a broad range of model eukaryotes. *J Biomol Screen* **19**: 379–386
- Attacha S, Solbach D, Bela K, Moseler A, Wagner S, Schwarzländer M, Aller I, Müller SJ, Meyer AJ (2017) Glutathione peroxidase-like enzymes cover five distinct cell compartments and membrane surfaces in *Arabidopsis thaliana*. *Plant Cell Environ* **40**: 1281–1295
- Bangash SAK, Müller-Schüssele SJ, Solbach D, Jansen M, Fiorani F, Schwarzländer M, Kopriva S, Meyer AJ (2019) Low-glutathione mutants are impaired in growth but do not show an increased sensitivity to moderate water deficit. *PLoS ONE* **14**: e0220589, doi: 10.1371/journal.pone.0220589
- Belousov VV, Fradkov AF, Lukyanov KA, Staroverov DB, Shakhbazov KS, Tersikh AV, Lukyanov S (2006) Genetically encoded fluorescent indicator for intracellular hydrogen peroxide. *Nat Methods* **3**: 281–286
- Bestetti S, Galli M, Sorrentino I, Pinton P, Rimessi A, Sitia R, Medrano-Fernandez I (2020) Human aquaporin-11 guarantees efficient transport of H_2O_2 across the endoplasmic reticulum membrane. *Redox Biol* **28**: 101326
- Bienert GP, Chaumont F (2014) Aquaporin-facilitated transmembrane diffusion of hydrogen peroxide. *Biochim Biophys Acta* **1840**: 1596–1604
- Bilan DS, Belousov VV (2018) *In vivo* imaging of hydrogen peroxide with HyPer probes. *Antioxid Redox Signal* **29**: 569–584
- Boisson-Dernier A, Lituiev DS, Nestorova A, Franck CM, Thirugnanarajah S, Grossniklaus U (2013) ANXUR receptor-like kinases coordinate cell wall integrity with growth at the pollen tube tip via NADPH oxidases. *PLoS Biol* **11**: e1001719

- Bratt A, Rosenwasser S, Meyer A, Fluhr R (2016) Organelle redox autonomy during environmental stress. *Plant Cell Environ* **39**: 1909–1919
- Caplan JL, Kumar AS, Park E, Padmanabhan MS, Hoban K, Modla S, Czymmek K, Dinesh-Kumar SP (2015) Chloroplast stromules function during innate immunity. *Dev Cell* **34**: 45–57
- Cejudo FJ, Ojeda V, Delgado-Requerey V, González M, Pérez-Ruiz JM (2019) Chloroplast redox regulatory mechanisms in plant adaptation to light and darkness. *Front Plant Sci* **10**: 380
- Chan KX, Phua SY, Crisp P, McQuinn R, Pogson BJ (2016) Learning the languages of the chloroplast: retrograde signaling and beyond. *Annu Rev Plant Biol* **67**: 25–53
- Chauvigné F, Boj M, Finn RN, Cerdà J (2015) Mitochondrial aquaporin-8-mediated hydrogen peroxide transport is essential for teleost spermatozoon motility. *Sci Rep* **5**: 7789
- Cochemé HM, Murphy MP (2008) Complex I is the major site of mitochondrial superoxide production by paraquat. *J Biol Chem* **283**: 1786–1798
- Costa A, Drago I, Behera S, Zottini M, Pizzo P, Schroeder JJ, Pozzan T, Lo Schiavo F (2010) H₂O₂ in plant peroxisomes: an *in vivo* analysis uncovers a Ca²⁺-dependent scavenging system. *Plant J Cell Mol Biol* **62**: 760–772
- Cui F, Brosché M, Shapiguzov A, He X-Q, Vainonen JP, Leppälä J, Trotta A, Kangasjärvi S, Salojärvi J, Kangasjärvi J, et al. (2019) Interaction of methyl viologen-induced chloroplast and mitochondrial signalling in *Arabidopsis*. *Free Radic Biol Med* **134**: 555–566
- De Col V, Fuchs P, Nietzel T, Elsässer M, Voon CP, Candeo A, Seeliger I, Fricker MD, Grefen C, Möller IM, et al. (2017) ATP sensing in living plant cells reveals tissue gradients and stress dynamics of energy physiology. *ELife* **6**: e26770
- Delanay A, Pflieger D, Barrault MB, Vinh J, Toledano MB (2002) A thiol peroxidase is an H₂O₂ receptor and redox-transducer in gene activation. *Cell* **111**: 471–481
- Dietz K-J, Turkan I, Krieger-Liszkay A (2016) Redox- and reactive oxygen species-dependent signaling into and out of the photosynthesizing chloroplast. *Plant Physiol* **171**: 1541–1550
- Dietz K-J, Wesemann C, Wegener M, Seidel T (2019) Toward an integrated understanding of retrograde control of photosynthesis. *Antioxid Redox Signal* **30**: 1186–1205
- Elsässer M, Feitosa-Araujo E, Lichtenauer S, Wagner S, Fuchs P, Giese J, Kotnik F, Hippler M, Meyer AJ, Maurino VG, et al. (2020) Photosynthetic activity triggers pH and NAD redox signatures across different plant cell compartments. *bioRxiv* 2020.10.31.363051
- Erickson JL, Kantek M, Schattat MH (2017) Plastid-nucleus distance alters the behavior of stromules. *Front Plant Sci* **8**: 1135
- Exposito-Rodriguez M, Laissue PP, Yvon-Durocher G, Smirnov N, Mullineaux PM (2017) Photosynthesis-dependent H₂O₂ transfer from chloroplasts to nuclei provides a high-light signalling mechanism. *Nat Commun* **8**: 49
- Fichman Y, Miller G, Mittler R (2019) Whole-plant live imaging of reactive oxygen species. *Mol Plant* **12**: 1203–1210
- Foyer CH, Noctor G (2005) Redox homeostasis and antioxidant signaling: a metabolic interface between stress perception and physiological responses. *Plant Cell* **17**: 1866–1875
- Fricker MD (2016) Quantitative redox imaging software. *Antioxid Redox Signal* **24**: 752–762
- Fufezan C, Rutherford AW, Krieger-Liszkay A (2002) Singlet oxygen production in herbicide-treated photosystem II. *FEBS Lett* **532**: 407–410
- Fujita M, Fujita Y, Iuchi S, Yamada K, Kobayashi Y, Urano K, Kobayashi M, Yamaguchi-Shinozaki K, Shinozaki K (2012) Natural variation in a polyamine transporter determines paraquat tolerance in *Arabidopsis*. *Proc Natl Acad Sci U S A* **109**: 6343–6347
- Gutschner M, Sobotta MC, Wabnitz GH, Ballikaya S, Meyer AJ, Samstag Y, Dick TP (2009) Proximity-based protein thiol oxidation by H₂O₂-scavenging peroxidases. *J Biol Chem* **284**: 31532–31540
- Haber Z, Rosenwasser S (2020) Resolving the dynamics of photosynthetically produced ROS by high-resolution monitoring of chloroplastic E_{GSH} in *Arabidopsis*. *bioRxiv* 2020.03.04.976092
- Jiang K, Schwarzer C, Lally E, Zhang S, Ruzin S, Machen T, Remington SJ, Feldman L (2006) Expression and characterization of a redox-sensing green fluorescent protein (reduction-oxidation-sensitive green fluorescent protein) in *Arabidopsis*. *Plant Physiol* **141**: 397–403
- Jung H-S, Crisp PA, Estavillo GM, Cole B, Hong F, Mockler TC, Pogson BJ, Chory J (2013) Subset of heat-shock transcription factors required for the early response of *Arabidopsis* to excess light. *Proc Natl Acad Sci U S A* **110**: 14474–14479
- Karimi M, Inzé D, Depicker A (2002) GATEWAY vectors for *Agrobacterium*-mediated plant transformation. *Trends Plant Sci* **7**: 193–195
- Krieger-Liszkay A (2005) Singlet oxygen production in photosynthesis. *J Exp Bot* **56**: 337–346
- Liebthal M, Maynard D, Dietz K-J (2018) Peroxiredoxins and redox signaling in plants. *Antioxid Redox Signal* **28**: 609–624
- Liu Z-J, Zhang X-L, Bai J-G, Suo B-X, Xu P-L, Wang L (2009) Exogenous paraquat changes antioxidant enzyme activities and lipid peroxidation in drought-stressed cucumber leaves. *Sci Hortic* **121**: 138–143
- Mangano S, Denita-Juarez SP, Marzol E, Borassi C, Estevez JM (2018) High auxin and high phosphate impact on RSL2 expression and ROS-homeostasis linked to root hair growth in *Arabidopsis thaliana*. *Front Plant Sci* **9**: 1164
- Marty L, Bausewein D, Müller C, Bangash SAK, Moseler A, Schwarzländer M, Müller-Schüssele SJ, Zechmann B, Riondet C, Balk J, et al. (2019) *Arabidopsis* glutathione reductase 2 is indispensable in plastids, while mitochondrial glutathione is safeguarded by additional reduction and transport systems. *New Phytol* **224**: 1569–1584
- Marty L, Siala W, Schwarzländer M, Fricker MD, Wirtz M, Sweetlove LJ, Meyer Y, Meyer AJ, Reichheld J-P, Hell R (2009) The NADPH-dependent thioredoxin system constitutes a functional backup for cytosolic glutathione reductase in *Arabidopsis*. *Proc Natl Acad Sci U S A* **106**: 9109–9114
- Meyer AJ, Brach T, Marty L, Kreye S, Rouhier N, Jacquot J-P, Hell R (2007) Redox-sensitive GFP in *Arabidopsis thaliana* is a quantitative biosensor for the redox potential of the cellular glutathione redox buffer. *Plant J* **52**: 973–986
- Meyer AJ, Dick TP (2010) Fluorescent protein-based redox probes. *Antioxid Redox Signal* **13**: 621–650
- Mhamdi A, Queval G, Chaouch S, Vanderauwera S, Van Breusegem F, Noctor G (2010) Catalase function in plants: a focus on *Arabidopsis* mutants as stress-mimic models. *J Exp Bot* **61**: 4197–4220
- Morgan B, Sobotta MC, Dick TP (2011) Measuring E_{GSH} and H₂O₂ with roGFP2-based redox probes. *Free Radic Biol Med* **51**: 1943–1951
- Morgan B, Van Laer K, Owusu TNE, Ezerija D, Pastor-Flores D, Amponsah PS, Tursch A, Dick TP (2016) Real-time monitoring of basal H₂O₂ levels with peroxiredoxin-based probes. *Nat Chem Biol* **12**: 437–443
- Mubarakshina MM, Ivanov BN, Naydov IA, Hillier W, Badger MR, Krieger-Liszkay A (2010) Production and diffusion of chloroplastic H₂O₂ and its implication to signalling. *J Exp Bot* **61**: 3577–3587
- Müller SM, Galliardt H, Schneider J, Barisas BG, Seidel T (2013) Quantification of Förster resonance energy transfer by monitoring sensitized emission in living plant cells. *Front Plant Sci* **4**: 413
- Müller-Schüssele SJ, Wang R, Gütle DD, Romer J, Rodriguez-Franco M, Scholz M, Buchert F, Lüth VM, Kopriva S, Dörmann P, et al. (2020) Chloroplasts require glutathione reductase to balance reactive oxygen species and maintain efficient photosynthesis. *Plant J* **103**: 1140–1154
- Murashige T, Skoog F (1962) A revised medium for rapid growth and bio assays with tobacco tissue cultures. *Physiol Plant* **15**: 473–497

- Narendra S, Venkataramani S, Shen G, Wang J, Pasapula V, Lin Y, Kornyejev D, Holaday AS, Zhang H (2006) The *Arabidopsis* ascorbate peroxidase 3 is a peroxisomal membrane-bound antioxidant enzyme and is dispensable for *Arabidopsis* growth and development. *J Exp Bot* **57**: 3033–3042
- Nietzel T, Elsässer M, Ruberti C, Steinbeck J, Ugalde JM, Fuchs P, Wagner S, Ostermann L, Moseler A, Lemke P, et al. (2019) The fluorescent protein sensor roGFP2-Orp1 monitors *in vivo* H₂O₂ and thiol redox integration and elucidates intracellular H₂O₂ dynamics during elicitor-induced oxidative burst in *Arabidopsis*. *New Phytol* **221**: 1649–1664
- Pak VV, Ezeriņa D, Lyublinskaya OG, Pedre B, Tyurin-Kuzmin PA, Mishina NM, Thauvin M, Young D, Wahni K, Gache SAM, et al. (2020) Ultrasensitive genetically encoded indicator for hydrogen peroxide identifies roles for the oxidant in cell migration and mitochondrial function. *Cell Metab* **31**: 642–653.e6
- Park S-W, Li W, Viehhauser A, He B, Kim S, Nilsson AK, Andersson MX, Kittle JD, Ambavaram MMR, Luan S, et al. (2013) Cyclophilin 20-3 relays a 12-oxo-phytodienoic acid signal during stress responsive regulation of cellular redox homeostasis. *Proc Natl Acad Sci U S A* **110**: 9559–9564
- Pérez-Sancho J, Tilsner J, Samuels AL, Botella MA, Bayer EM, Rosado A (2016) Stitching organelles: organization and function of specialized membrane contact sites in plants. *Trends Cell Biol* **26**: 705–717
- Perico C, Sparkes I (2018) Plant organelle dynamics: cytoskeletal control and membrane contact sites. *New Phytol* **220**: 381–394
- Queval G, Hager J, Gakière B, Noctor G (2008) Why are literature data for H₂O₂ contents so variable? A discussion of potential difficulties in the quantitative assay of leaf extracts. *J Exp Bot* **59**: 135–146
- Rodrigues O, Reshetnyak G, Grondin A, Saijo Y, Leonhardt N, Maurel C, Verdoucq L (2017) Aquaporins facilitate hydrogen peroxide entry into guard cells to mediate ABA- and pathogen-triggered stomatal closure. *Proc Natl Acad Sci U S A* **114**: 9200–9205
- Rosenwasser S, Rot I, Meyer AJ, Feldman L, Jiang K, Friedman H (2010) A fluorometer-based method for monitoring oxidation of redox-sensitive GFP (roGFP) during development and extended dark stress. *Physiol Plant* **138**: 493–502
- Rosenwasser S, Rot I, Sollner E, Meyer AJ, Smith Y, Leviatan N, Fluhr R, Friedman H (2011) Organelles contribute differentially to reactive oxygen species-related events during extended darkness. *Plant Physiol* **156**: 185–201
- Rossel JB, Wilson PB, Hussain D, Woo NS, Gordon MJ, Mewett OP, Howell KA, Whelan J, Kazan K, Pogson BJ (2007) Systemic and Intracellular Responses to Photooxidative Stress in *Arabidopsis*. *Plant Cell* **19**: 4091–4110
- Scarpeci TE, Zanol MI, Carrillo N, Mueller-Roeber B, Valle EM (2008) Generation of superoxide anion in chloroplasts of *Arabidopsis thaliana* during active photosynthesis: a focus on rapidly induced genes. *Plant Mol Biol* **66**: 361–378
- Schindelin J, Arganda-Carreras I, Frise E, Kaynig V, Longair M, Pietzsch T, Preibisch S, Rueden C, Saalfeld S, Schmid B, et al. (2012) Fiji: an open-source platform for biological-image analysis. *Nat Methods* **9**: 676–682
- Schöttler MA, Tóth SZ (2014) Photosynthetic complex stoichiometry dynamics in higher plants: environmental acclimation and photosynthetic flux control. *Front Plant Sci* **5**: 188
- Schuller JM, Birrell JA, Tanaka H, Konuma T, Wulffhorst H, Cox N, Schuller SK, Thiemann J, Lubitz W, Sétif P, et al. (2019) Structural adaptations of photosynthetic complex I enable ferredoxin-dependent electron transfer. *Science* **363**: 257–260
- Schwarzländer M, Dick TP, Meyer AJ, Morgan B (2016) Dissecting redox biology using fluorescent protein sensors. *Antioxid Redox Signal* **24**: 680–712
- Schwarzländer M, Fricker MD, Müller C, Marty L, Brach T, Novak J, Sweetlove LJ, Hell R, Meyer AJ (2008) Confocal imaging of glutathione redox potential in living plant cells. *J Microsc* **231**: 299–316
- Schwarzländer M, Fricker MD, Sweetlove LJ (2009) Monitoring the *in vivo* redox state of plant mitochondria: effect of respiratory inhibitors, abiotic stress and assessment of recovery from oxidative challenge. *Biochim Biophys Acta* **1787**: 468–475
- Schwarzländer M, Wagner S, Ermakova YG, Belousov VV, Radi R, Beckman JS, Buettner GR, Demarex N, Duchon MR, Forman HJ, et al. (2014) The “mitoflash” probe cpYFP does not respond to superoxide. *Nature* **514**: E12–E14
- Sewelam N, Jaspert N, Van Der Kelen K, Tognetti VB, Schmitz J, Frerigmann H, Stahl E, Zeier J, Van Breusegem F, Maurino VG (2014) Spatial H₂O₂ signaling specificity: H₂O₂ from chloroplasts and peroxisomes modulates the plant transcriptome differentially. *Mol Plant* **7**: 1191–1210
- Shameer S, Ratcliffe RG, Sweetlove LJ (2019) Leaf energy balance requires mitochondrial respiration and export of chloroplast NADPH in the light. *Plant Physiol* **180**: 1947–1961
- Shapiguzov A, Vainonen JP, Hunter K, Tossavainen H, Tiwari A, Järvi S, Hellman M, Aarabi F, Alseekh S, Wybouw B, et al. (2019) *Arabidopsis* RCD1 coordinates chloroplast and mitochondrial functions through interaction with ANAC transcription factors. *eLife* **8**: e43284
- Smirnov N, Arnaud D (2019) Hydrogen peroxide metabolism and functions in plants. *New Phytol* **221**: 1197–1214
- Sobotta MC, Barata AG, Schmidt U, Mueller S, Millonig G, Dick TP (2013) Exposing cells to H₂O₂: a quantitative comparison between continuous low-dose and one-time high-dose treatments. *Free Radic Biol Med* **60**: 325–335
- de Souza A, Wang J-Z, Dehesh K (2017) Retrograde signals: integrators of interorganellar communication and orchestrators of plant development. *Annu Rev Plant Biol* **68**: 85–108
- Speiser A, Silberman M, Dong Y, Haberland S, Uslu VV, Wang S, Bangash SAK, Reichelt M, Meyer AJ, Wirtz M, et al. (2018) Sulfur partitioning between glutathione and protein synthesis determines plant growth. *Plant Physiol* **177**: 927–937
- Sylvestre-Gonon E, Law SR, Schwartz M, Robe K, Keech O, Didierjean C, Dubos C, Rouhier N, Hecker A (2019) Functional, structural and biochemical features of plant serinyl-glutathione transferases. *Front Plant Sci* **10**: 608
- Teicher BH, Scheller VH (1998) The NAD(P)H dehydrogenase in barley thylakoids is photoactivatable and uses NADPH as well as NADH. *Plant Physiol* **117**: 525–532
- Uehlein N, Otto B, Hanson DT, Fischer M, McDowell N, Kaldenhoff R (2008) Function of *Nicotiana tabacum* aquaporins as chloroplast gas pores challenges the concept of membrane CO₂ permeability. *Plant Cell* **20**: 648–657
- Ugalde JM, Fecker L, Schwarzländer M, Müller-Schüssele SM, Meyer AJ (2020a) Live monitoring of ROS-induced cytosolic redox changes with roGFP2-based sensors in plants. *bioRxiv* 2020.12.21.423768
- Ugalde JM, Lamig L, Herrera-Vásquez A, Fuchs P, Müller-Schüssele SJ, Meyer AJ, Holuigue L (2020b) GSTU7 affects growth performance and acts as an antagonist of oxidative stress induced by methyl viologen. *bioRxiv* 2020.06.09.142729
- Van Aken O, Ford E, Lister R, Huang S, Millar AH (2016) Retrograde signalling caused by heritable mitochondrial dysfunction is partially mediated by ANAC017 and improves plant performance. *Plant J Cell Mol Biol* **88**: 542–558
- Wagner S, Steinbeck J, Fuchs P, Lichtenauer S, Elsässer M, Schippers JHM, Nietzel T, Ruberti C, Van Aken O, Meyer AJ, et al. (2019) Multiparametric real-time sensing of cytosolic physiology links hypoxia responses to mitochondrial electron transport. *New Phytol* **224**: 1668–1684
- Waszczak C, Carmody M, Kangasjärvi J (2018) Reactive oxygen species in plant signaling. *Annu Rev Plant Biol* **69**: 209–236
- Xi J, Xu P, Xiang C-B (2012) Loss of AtPDR11, a plasma membrane-localized ABC transporter, confers paraquat tolerance in *Arabidopsis thaliana*. *Plant J Cell Mol Biol* **69**: 782–791